WORLD JOURNAL OF PHARMACEUTICAL RESEARCH
SJIF Impact Factor 7.523
Volume 7, Issue 03, 1260-1277. Research Article ISSN 2277–7105

WASTEWATER DISINFECTION BY INSITU HYDROTHERMAL SYNTHESIS OF RGO SUPPORTED MoO_3/Fe_2O_3 TERNARY NANOCOMPOSITE

R. Balaji Anjaneyulu[a*], B. Sathish Mohan[b], G. Parasuram Naidu[a], M. Jagadeesh Babu[a], S. Jhansi Rani[a] and R. Muralikrishna[a]

[a]Dept of Physical, Nuclear Chemistry and Chemical Oceanography, Andhra University, Visakhapatnam-530003, India.

[b]Dept of Inorganic and Analytical Chemistry, Andhra University, Visakhapatnam-530003, India.

Article Received on
18 Dec. 2017,
Revised on 07 Jan. 2018,
Accepted on 28 Jan. 2018
DOI: 10.20959/wjpr20183-10974

***Corresponding Author**
Dr. R. Balaji Anjaneyulua
Dept of Physical, Nuclear Chemistry and Chemical Oceanography, Andhra University, Visakhapatnam-530003, India.

ABSTRACT

An attempt to evaluate the antibacterial activity of reduced graphene oxide supported ternary nanocomposite (MoO_3/Fe_2O_3/RGO), which was studied its structural and morphological studies by X-ray diffraction (XRD), Fourier transform infrared (FTIR), Scanning electron microscopy (FESEM-EDX), N_2 adsorption-desorption isotherm (BET) and UV-Visible spectrophotometer. This ternary nanocomposite, has a good potent for antibacterial activity against on both Gram positive bacteria (*Bacillus subtilis* and *Escherichia coli*) and Gram negative bacteria (*Staphylococcus aureus* and *Pseudomonas aeruginosa*).

KEYWORDS: MoO_3/Fe_2O_3/RGO, *Bacillus subtilis* and *Escherichia coli*, *Staphylococcus aureus* and *Pseudomonas aeruginosa.*

1. INTRODUCTION

Due to increase the large population, industrialization, urbanization and some traditional chemical disinfectants (free chlorine, chloramines and ozone) pollutes the water. Besides, the conflict of microorganisms to the common chemical disinfectants are increasing, consequently greater alternatives are necessary. The removal of bacteria from water is an extremely important process for drinking and sanitation systems especially against concerns

on growing outbreaks of water borne diseases.[1,2] Current advances in the field of nanobiotechnology, particularly inorganic materials with a high antimicrobial efficiency are important tools to prevent the growth, spread and transfer of harmful and noxious microorganisms. They actively disable pathologically relevant bacteria in order to reduce the transmission of infection in public and health care environments.

Controlled syntheses of metal oxide nanoparticles are essential for several applications and solution phase method provides a large degree of control over the synthesis products[3] which are found to be a good inhibitor of different bacterial strains.[4-6] Molybdenum trioxide and its hydrated components exhibit several stable and metastable crystalline polymorphs including orthorhombic, monoclinic and hexagonal phases.[7,8] Molybdenum trioxide crystals have a wide range of applications as industrial catalysts[9] electro-photochromic materials.[10–12] The antimicrobial activity of molybdenum trioxide and related materials has only been reported recently.[13–17] Extensive studies are available, which suggests that highly active metal, metal oxide, metal oxide composite nanoparticles exhibit excellent antimicrobial properties.[18-23] But there are several disadvantages of these materials such as high cost for their preparation, low-active surface area and high cytotoxicity are major constraints limiting their application[24-25] Therefore, recent research work focuses metal oxides, metal composites and metal oxides mixed with suitable support to increases their antibacterial agent properties.

Recently, many reports have been reported on graphene-based materials for promising antibacterial materials.[26–30] The auspicious blend of physical structure and chemical functionality was determined by of GO and RGO antibacterial activity.[31] Reduced graphene oxide (graphene) is a single layer of carbon densely packed in a honeycomb crystal lattice structure and as the presence of a perfect 2-D single layer of sp^2 hybridized carbon atom. Its remarkable properties are large surface area (2630 m^2/g), zero band-gap, high transmittance rate of visible and UV lights, high thermal conductivity, good chemical stability and corrosion resistance imply that it can be used as an excellent adsorbent.[32-35] Upon contact with such a nanostructure, membrane stress induced by the sharp edges of graphene nanosheets has been appeared to make huge physical damage to cell membrane, and resulting loss of bacterial membrane reliability and leakage of intracellular material.[36]

Hence considering above issues, we have attempted to prepare a cost-effective, RGO supported ternary nanocomposite via hydrothermal process in order to get synergistic effect towards the enhancive antibacterial activity towards various Gram positive bacteria (*Bacillus*

subtilis and *Escherichia coli*) and Gram negative bacteria (*Staphylococcus aureus* and *Pseudomonas aeruginosa*).

2. MATERIALS AND METHODS

2.1. Materials

Pure and analytical grade chemicals were used in all experiments including synthesis of nanoparticles and media preparation for growth of bacterial cells. Graphite powder, Hydrogen peroxide (H_2O_2) (30%), Hydrochloric acid (HCl) (36.5%), Sulfuric acid (H_2SO_4) (98%), Potassium permanganate ($KMnO_4$), Sodium nitrite ($NaNO_3$), Nitric acid (HNO_3) (69%) and Sodium hydroxide (NaOH) were purchased from Merck Chemicals Pvt. Ltd, India. Ammonium heptamolybdate tetrahydrate ($(NH_4)_6Mo_7O_{24}.4H_2O$) was obtained from Sigma Aldrich Chemicals Pvt. Ltd, India. Triton$^{@}$X-100 (TX-100) were procured from Rankem Chemicals Pvt. Ltd, India. Nutrient Agar, Peptone, Beef extract, Agar-agar, Nutrient broth, Ethanol, Dimethylsulphoxide (DMSO), Neomycin (Broad spectrum antibiotic) were purchased from Himedia, Mumbai, India. The microbial strains, *Bacillus subtilis*, *Escherichia coli*, Staphylococcus *aureus* and *Pseudomonas aeruginosa* were collected from Microbial Type Culture Collection, Institute of Microbial Technology and Chandigarh.

2.2 Synthesis of MoO_3/Fe_2O_3/RGO ternary nanocomposite

Synthesis of α-MoO_3 nanobelts

In a typical synthesis, 1.5 g of ammonium heptamolybdate tetrahydrate ($(NH_4)_6Mo_7O_{24}.4H_2O$) was dissolved in 39 mL of distilled water under magnetic stirring. Then, 21 mL of 3 mol L^{-1} HNO_3 was added to the above solution, stirring for 5 min and then 100 µL TX-100 was slowly added dropwise to the above solution. The obtained transparent solution was transferred and sealed in a Teflon-lined stainless autoclave with a capacity of 100 mL. The autoclave was heated to 180^{o}C for 20 h in an oven. After completion of 20 h reaction, the autoclave was allowed to cool, to attain room temperature. The obtained precipitate was washed several times with absolute ethanol and double distilled water and then dried at 60^{o}C for overnight.

Synthesis of MoO_3/Fe_2O_3 binary nanocomposite

For the formation of MoO_3/Fe_2O_3 binary nanocomposite, 0.5 g of MoO_3 nanobelts powder was added to 50 mL of 0.01 mol L^{-1} $Fe(NO_3)_3.9H_2O$ of ethanol solution. After 2 h stirring, the mixture was transferred and sealed in a Teflon-lined stainless autoclave with a capacity of

100 mL and autoclave was kept at 180^{o}C for 24 h in temperature controlled oven. After 20 h reaction, the autoclave was allowed to cool till room temperature; finally the obtained product was washed with 2D water and dried at 60^{o}C for overnight.

Synthesis of MoO_3/Fe_2O_3/RGO ternary nanocomposite

Graphene oxide (GO) was synthesized by a modified Hummer's method.[37] For the synthesis of MoO_3/Fe_2O_3/RGO ternary nanocomposite, the prepared calculated amount (5 Wt%) of GO was sonicated in 50 mL 2D water for 1 h to generate a clear brown dispersion and then, 0.5 g of MoO_3/Fe_2O_3 binary nanocomposite powder was added. The mixture was vigorously stirred for 2 h to obtained homogeneous solution. The obtained resulting solution was transferred into a Teflon-lined stainless 100 mL capacity of autoclave and maintained at 180^{o}C for 24 h in temperature controlled oven. After 24 h reaction, the autoclave was allowed to cool till room temperature; finally the obtained product was washed and then dried at 60^{o}C for overnight.

2.3. Instrumentation

The prepared samples were characterized using Powder X-ray diffraction (XRD) (D8-Focus, Bruker instrument, Germany) with Cu Kα radiation (λ=1.5406 A^{o}), 2θ ranges from 10 to 90^{o} with scanning speed of 0.02^{o} S^{-1} to identify the crystalline phase of samples. FTIR (IFS-66/S, Bruker instrument, Germany) were performed in the transmittance mode, 400–4000 cm^{-1} spectral range with a resolution greater than 0.1 cm^{-1}. Surface morphology and elemental analysis was performed using a Quanta FEG 450 scanning electron microscopy (FESEM) and energy dispersive X-ray (EDX) spectrophotometer. The band gap was calculated using UV-Visible absorption spectra from UV-DRS spectrophotometer (UV-2600R, Shimadzu, Japan). Brunauer-Emmett-Teller (BET) (Quantachrome Nova 2200 E) surface area was determined from the N_2 adsorption-desorption isotherm at 77.3 K.

2.4. Investigation of antibacterial activity

Preparation of media (Nutrient agar) for bacteria

The ingredients (Peptone, Yeast extract, NaCl and Agar-agar) were mixed and dissolved by heating and pH was adjusted to 7.5 ± 0.1. The broth was solidified by adding agar and sterilized by autoclaving at 121^{o}C for 15 min and poured into sterile petri dishes and the media was preserved in refrigerator for further use.

Determination of antibacterial activity of prepared nanocomposite

Active cultures were generated by inoculating a loopful of culture in separate 100 mL nutrient/potato dextrose broths and incubating on a shaker at 37^{o}C on overnight. The cells were harvested by centrifuging at 4000 rpm for 5 min, washed with normal saline, spun at 4000 rpm for 5 min again and diluted in normal saline to obtain 5x10^{5} CFU/mL.

Synthesized nanocatalysts were subjected to antibacterial assay using the agar well diffusion method.[38,39] Nutrient agar (20 mL) was dispensed into sterile universal bottles, these were then inoculated with 0.2 mL of cultures, mixed gently and poured into sterile petri dishes. After setting, a number 3-cup borer (6 mm) diameter was properly sterilized by flaming and used to make four uniform wells in each petri dish. The wells were filled with DMSO containing catalyst (1 mg/mL) and allowed for diffusion for 45 min. The plates were incubated at 37 ^{o}C for 24 h for bacteria. Neomycin was included in the positive control and DMSO as negative control. The inhibition zones were measured with antibiotic zone scale in mm and the experiment was carried out in triplicates.

Minimum inhibitory concentration (MIC) assays

Minimum inhibitory concentrations (MIC) of nanocatalysts were determined according to the method.[40] A series of two fold dilution of nanocatalysts, ranging from 100-2000 µg/mL, were prepared. After sterilization, the medium was inoculated with the aliquots of culture containing approximately 5×10^{5} CFU/mL of each organism of 24 h slant culture in aseptic condition and transferred into sterile 6 inch diameter petri dishes and allowed to set at room temperature for about 10 min and then kept in a refrigerator for 30 min. After the media was solidified, wells were made and different concentrations of compounds ranging from 100-2000 µg/mL were added to the wells of each petri dish. The blank plates were carried without nanocatalysts. Inhibition of the growth of the organism in the plates containing nanocatalysts was judged by comparison with the growth in the control plates. The MICs were determined as the lowest concentration of the nanocatalyst inhibiting visible growth of each organism on the agar plate.

3. RESULTS AND DISCUSSION

The X-ray power diffraction pattern of the prepared catalysts, MoO_3, MoO_3/Fe_2O_3 and MoO_3/Fe_2O_3 nanocomposites with content of RGO (Fig.3.1.A). Fig.3.1.A. (a) shows the diffraction peaks at 2θ = 11^{o} and 43^{o}, attributes to (002) and (100) reflections respectively,

resultant phase of GO.[41] Fig.3.1.A. (b) shows the XRD patterns of prepared MoO_3 nanobelts, indicating the presence of sharp diffraction peaks found at 2θ = 12.81°, 23.47°, 25.80°, 27.36°, 29.54°, 33.73°, 35.61°, 39.06°, 46.30° and 49.34° were assigned to the (020), (110), (040), (021), (130), (111), (041), (060), (200) and (002) reflection lines respectively, which are closely matched with the reflection lines of α-MoO_3, compared with Standard JCPDS (File No. 05-0508).[42] This result shows that there is no impurity peaks any in the XRD pattern, leads to formation of high pure orthorhombic α-MoO_3 using hydrothermal approach. All the peaks related to α-MoO_3 crystal phase remain prominently appeared after coupling with Fe_2O_3 (Fig.3.1.A. (c)), but Fe_2O_3 diffraction peaks (standard JPCDS File No. 33-0664) has been appear with very low intensity due to relatively small amount of Fe_2O_3 presented in MoO_3/Fe_2O_3 binary nanocomposite, which indicates the formation of a two-phase MoO_3/Fe_2O_3 binary nanocomposite. Further, the diffraction peaks of ternary nanocomposite shift slightly towards lower angles on RGO addition, as shown in Fig.3.1.A. (d). Moreover, the intensity of diffraction peaks decrease and the peaks width broadens as the amount of RGO increases, indicating the interactions of RGO in the ternary nanocomposite. No other diffraction peaks were observed in this pattern, indicating that pure phase occurred during the synthesis process. The average crystallite size was calculated using Debye Scherrer equation. While compare with the binary nanocomposite (31.8 nm) and MoO_3 (44.67 nm), the size of ternary nanocomposite to be low (22.3 nm), due to incorporation of RGO to the formation of ternary nanohybrid by hydrothermal assisted synthesis.

FTIR spectroscopy was used to investigation of existence of oxygen containing functionalities and changes after impregnation. Fig.3.1.B shows the FTIR spectra of GO, MoO_3, MoO_3/Fe_2O_3 and MoO_3/Fe_2O_3/RGO ternary nanocomposite. In Fig.3.1.B. (a) shows GO FTIR spectrum, the observed peaks at 1717.5 cm^{-1} and 1586 cm^{-1} could be attributed to C=O group and aromatic C=C group of GO. The hydroxyl (-OH) group exhibit broad band centered around 3235.5 cm^{-1}.[43,44] Carboxy (C-O), epoxy (C-O) and alkoxy (C-O) group peaks were at 1385.3 cm^{-1}, 1219.5 cm^{-1} and 1038.7 cm^{-1} respectively. The Fig.3.1.B. (b-d) shows MoO_3, MoO_3/Fe_2O_3 and MoO_3/Fe_2O_3/RGO ternary nanocomposite. FTIR spectra, all are having metal oxide stretching bands peaks between 1000 to 400 cm^{-1}. The FTIR spectrum of MoO_3/Fe_2O_3/RGO ternary nanocomposite reveals that the C=O and O-H group intensities decrease, which indicates the removal of oxygen containing groups through the employed synthesis method and high intensity peak observed at 1555.6 cm^{-1} for C=C bond, this results indicating that GO has been reduced to RGO via hydrothermal process.

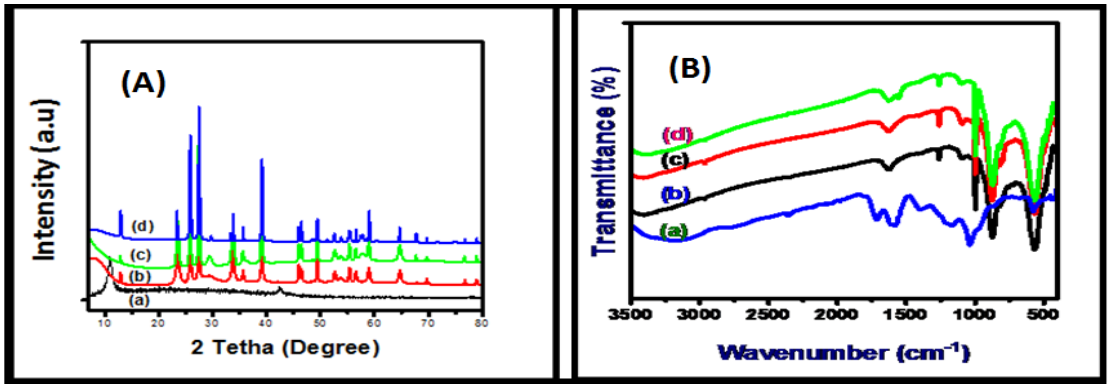

Fig.3.1.A. XRD Spectra of (a) Graphene oxide, (b) MoO_3, (c) MoO_3/Fe_2O_3 and (d) MoO_3/Fe_2O_3/RGO.

B. FT-IR spectra of (a) GO, (b) MoO_3, (c) MoO_3/Fe_2O_3 and (d) MoO_3/Fe_2O_3/RGO.

The morphological study of nanocomposite using FESEM and TEM (Fig.3.2). It can be obviously seen from Fig.3.2. (a) reveals a regularly uniform belt type structure of MoO_3 with relatively smooth surface. Fig.3.2. (b) shows FESEM images of MoO_3/Fe_2O_3 binary nanocomposite and the MoO_3 nanobelt particles were covered by large quantity of composite, it is evident that MoO_3 nanobelt type particles are embedded by Fe_2O_3 and form new MoO_3/Fe_2O_3 binary nanocomposite as explained in XRD results (Fig.3.1.A. (c)). Fig.3.2. (c) shows the surface morphology of ternary nanocomposite. The elemental composition of the ternary nanocomposite was determined using energy-dispersive X-ray spectroscopy (EDX) (Fig.3.2 (d)), which indicates the presence of Mo, Fe, O and C without impurities, evident that the formation of pure phase ternary nanocomposite, were in support of the XRD results which confirm the purity of ternary nanocomposite structure.

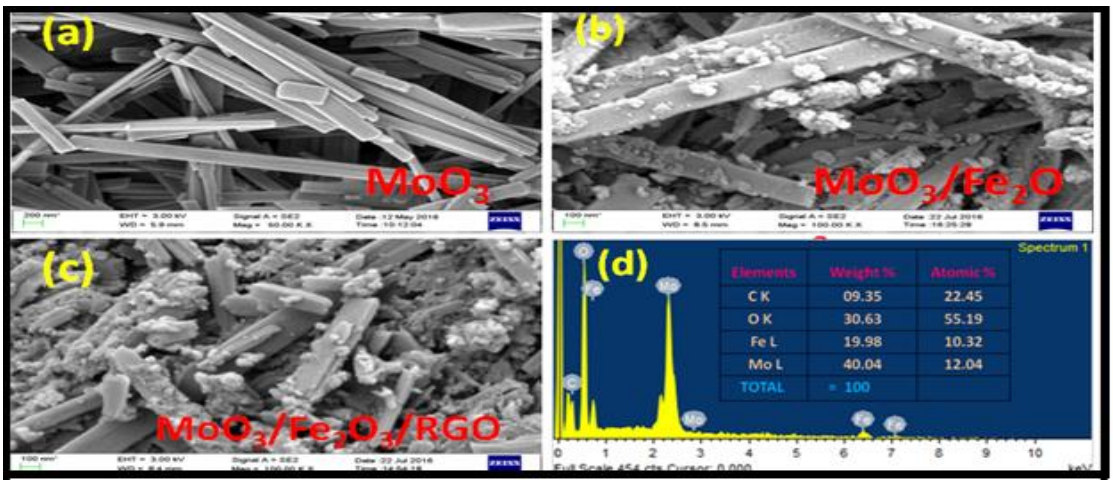

Fig.3.2. FESEM images of (a) MoO_3, (b) MoO_3/Fe_2O_3, (c) MoO_3/Fe_2O_3/RGO and (d) EDX image of MoO_3/Fe_2O_3/RGO.

The light- absorbance properties of as prepared catalysts were measured using UV−Vis diffuse reflectance spectroscopy (UV-DRS), which interprets the band gap energies of nanocomposite can be calculated using the following formula.[45]

$$E_g\ (eV) = \frac{1240}{\lambda}$$

Where, E_g is band gap energy, λ is wavelength (nm) corresponding to the absorption edge.

The band gap energies (E_g) of pure MoO_3, MoO_3/Fe_2O_3 nanocomposite and MoO_3/Fe_2O_3/RGO ternary nanocomposite were calculated to be 2.88 (430 nm), 1.76 (704 nm) and 1.65 (751) eV respectively (Fig 3.3). On the other hand, the absorption edge of the binary nanocomposite (MoO_3/Fe_2O_3), as shown in Fig.3.3 (b), shifts to the more visible range and has higher absorption intensity than pure MoO_3 (Fig.3.3 (a)), indicating the effective surface hybridization between these components.[46,47] For the ternary nanocomposite (Fig.3.3 (c)), with rGO loading, reaches a maximum absorption edge (751 nm). This evident that there exists an interaction of Mo–O–C and Fe–O–C in the ternary nanocomposite. Similar observation was reported earlier for semiconductors coupled with GO.[48,49] Thus, it can be confirmed that composite transition metal oxides and synergizing with rGO were efficient for visible-light response.

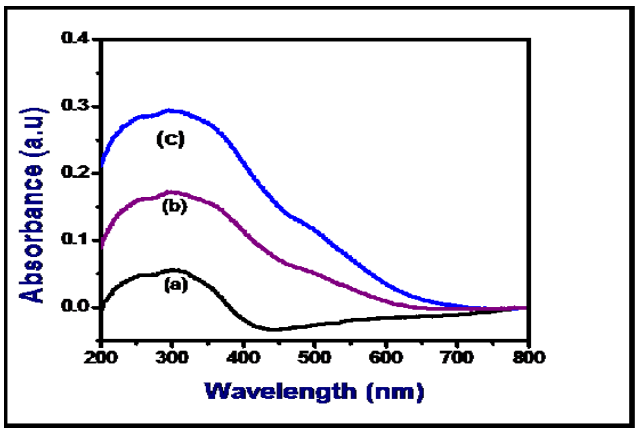

Fig.3.3.UV-Vis DRS spectra of (a) MoO_3, (b) MoO_3/Fe_2O_3 and (c) MoO_3/Fe_2O_3/RGO.

The specific surface area of as prepared catalysts were evaluated using N_2 adsorption–desorption analysis. The large surface area of nanocomposite can enhance the catalytic activity due to more active sites on the surface for the adsorption of reactant molecules. Table.3.1 shows the typical N_2 adsorption-desorption isotherms for MoO_3, MoO_3/Fe_2O_3 and MoO_3/Fe_2O_3/RGO having RGO containing ternary nanocomposite. Based on these results,

the specific surface areas of pure MoO_3, binary nanocomposite (MoO_3/Fe_2O_3) and the ternary nanocomposite (MoO_3/Fe_2O_3/RGO) are 9.0 m^2/g, 18.1m^2/g and 26.4 m^2/g. The higher specific surface area containing ternary nanocomposite (MoO_3/Fe_2O_3/RGO) is more active catalyst due to reactant molecule spend more time at surface of the catalyst and more number of molecules reacts with photoactive radicals in presence of visible light.

Table.3.1. The specific surface area of as prepared catalysts.

S.No	Catalyst	Specific surface area (m^2/g)
1	MoO_3	9.0
2	MoO_3/Fe_2O_3	18.1
3	MoO_3/Fe_2O_3/RGO	26.4

4. Investigation of wastewater disinfection

Antibacterial activity of MoO_3 nanobelts

The antibacterial properties of the MoO_3 nanobelts was evaluated against two Gram positive and two Gram negative bacterial strains using agar well diffusion method (Fig.3.4). Table.3.2 implies the inhibition zone and MIC of MoO_3 nanobelts on the growth of both Gram positive and Gram negative bacteria. Of the bacterial strains tested at the concentration of 25 µg and 50 µg, MoO_3 moderately inhibited the growth of Gram negative bacteria - *Escherichia coli* (18 mm) and *Pseudomonas aeruginosa* (23 mm) than Gram positive bacteria (strongly inhibited) - *Bacillus subtilis* (16 mm) and *Staphylococcus aureus* (14 mm) at a concentration of 50 µg and the MIC of MoO_3 for *Bacillus subtilis, Staphylococcus aureus, Escherichia coli* and *Pseudomonas aeruginosa* were intended, 0.70 mg/mL, 0.80 mg/mL, 0.80 mg/mL and 0.85 mg/mL respectively. MoO_3 showed a significant antibacterial activity on Gram positive and Gram negative bacterial strains.

Table.3.2. Shows the zone of inhibition and MIC of MoO_3 nanobelts on the growth of bacteria.

Name of the bacterial strain	Diameter of zone of inhibition (mm)			Minimum inhibitory concentration (MIC)
	MoO_3 nanobelts		Neomycin (20 µg)	
	25 µg	50 µg		
Gram positive				
Bacillus subtilis	9	16	28	0.70 mg/mL
Staphylococcus aureus	8	14	27	0.80 mg/mL
Gram negative				
Escherichia coli	11	18	28	0.80 mg/mL
Pseudomonas aeruginosa	11	23	28	0.85 mg/mL

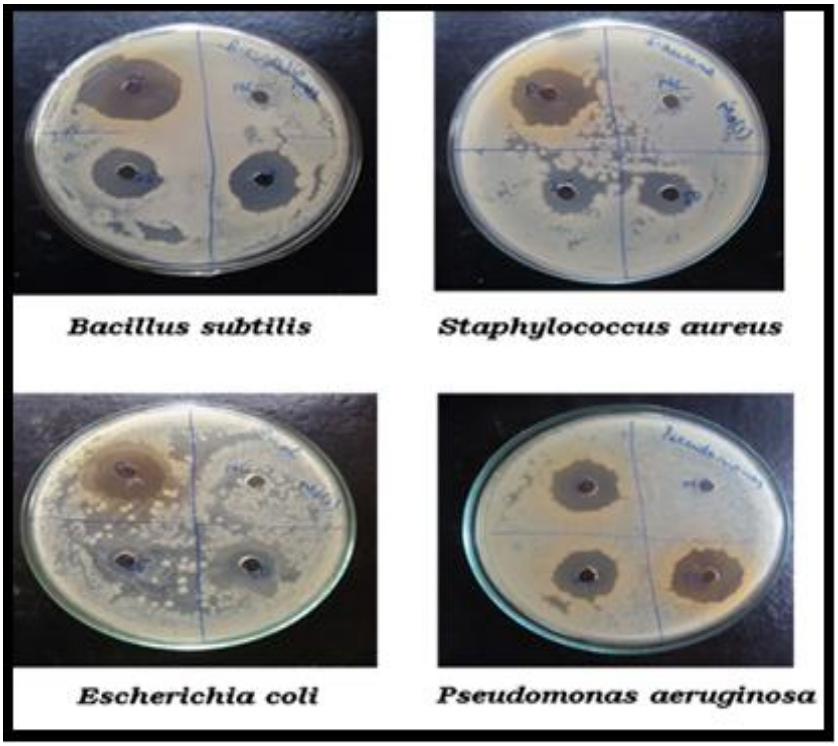

Fig.3.4. Antibacterial activity of MoO_3 nanobelts.

Antibacterial activity of MoO_3/Fe_2O_3 nanocomposite

Fig.3.5 shows the antibacterial properties of MoO_3/Fe_2O_3 nanocomposite was evaluated against two Gram positive and two Gram negative bacterial strains using agar well diffusion method. Table.3.3 shows the inhibition zone and MIC of MoO_3/Fe_2O_3 nanocomposite on the growth of both Gram positive and Gram negative bacteria. These results suggested that MoO_3/Fe_2O_3 showed significant antibacterial activity on Gram positive and Gram negative bacterial strains. Of the bacterial strains tested at two different concentrations 25 µg and 50 µg, MoO_3/Fe_2O_3 strongly inhibited the growth of Gram positive bacteria - *Bacillus subtilis* (18 mm) and *Staphylococcus aureus* (16 mm) at a concentration of 50 µg. On the other hand, MoO_3/Fe_2O_3 moderately inhibited the growth of Gram negative bacteria - *Escherichia coli* (19 mm) and *Pseudomonas aeruginosa* (24 mm) at a concentration of 50 µg tested. The MIC of MoO_3/Fe_2O_3 for *Bacillus subtilis, Staphylococcus aureus, Escherichia coli* and *Pseudomonas aeruginosa* were found to be 0.65 mg/mL, 0.75 mg/mL, 0.80 mg/mL and 0.80 mg/mL respectively.

Table.3.3: Shows the zone of inhibition and MIC of MoO_3/Fe_2O_3 nanocomposite on the growth of bacteria.

Name of the bacterial strain	Diameter of zone of inhibition (mm)			Minimum inhibitory concentration (MIC)
	MoO_3/Fe_2O_3 nanocomposite		Neomycin (20 µg)	
	25 µg	50 µg		
Gram positive				
Bacillus subtilis	10	18	28	0.65 mg/mL
Staphylococcus aureus	9	16	27	0.75 mg/mL
Gram negative				
Escherichia coli	10	19	28	0.80 mg/mL
Pseudomonas aerugunosa	12	24	26	0.80 mg/mL

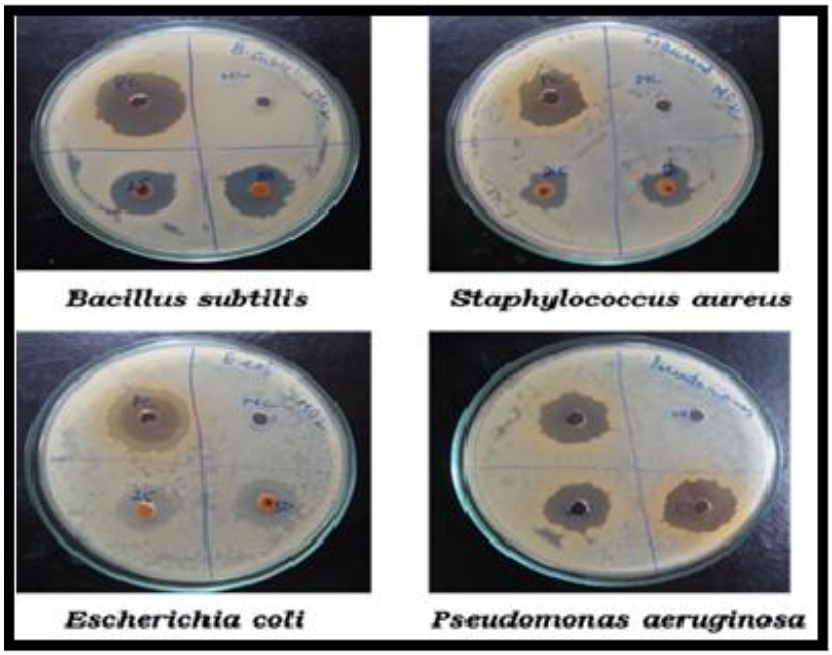

Fig.3.5. Antibacterial activity of MoO_3/Fe_2O_3 nanocomposite.

Antibacterial activity of MoO_3/Fe_2O_3/RGO nanocomposite

The antibacterial properties of MoO_3/Fe_2O_3/RGO ternary nanocomposite was evaluated against two Gram positive and two Gram negative bacterial strains using agar well diffusion method (Fig.3.6). Table.3.4 presents the zone of inhibition and MIC of MoO_3/Fe_2O_3/RGO nanocomposite on the growth of both Gram positive and Gram negative bacteria. Of the bacterial strains tested at concentrations of 25 µg and 50 µg, MoO_3/Fe_2O_3/RGO strongly inhibited the growth of Gram positive bacteria - *Bacillus subtilis* (25 mm) and *Staphylococcus aureus* (24 mm) at a concentration of 50 µg tested with similar to Gram negative bacteria - *Escherichia coli* (26 mm) and *Pseudomonas aeruginosa* (25 mm) at a concentration of 50 µg tested and the minimum inhibitory concentration (MIC) of

MoO_3/Fe_2O_3/RGO for *Bacillus subtilis*, *Staphylococcus aureus*, *Escherichia coli* and *Pseudomonas aeruginosa* were measured 0.60 mg/mL, 0.70 mg/mL, 0.65 mg/mL and 0.70 mg/mL respectively. Hence, these results declared that MoO_3/Fe_2O_3/RGO showed a potent antibacterial activity on both Gram positive and Gram negative bacterial strains.

Table.3.4. Shows the zone of inhibition and MIC of MoO_3/Fe_2O_3/RGO nanocomposite on the growth of bacteria.

Name of the bacterial strain	Diameter of zone of inhibition(mm)			Minimum inhibitory concentration (MIC)
	MoO_3/Fe_2O_3/RGO nanocomposite		Neomycin (20 µg)	
	25 µg	50 µg		
Gram positive				
Bacillus subtilis	12	25	28	0.60 mg/mL
Staphylococcus aureus	12	24	28	0.70 mg/mL
Gram negative				
Escherichia coli	13	26	27	0.65 mg/mL
Pseudomonas aerugunosa	12	25	28	0.70 mg/mL

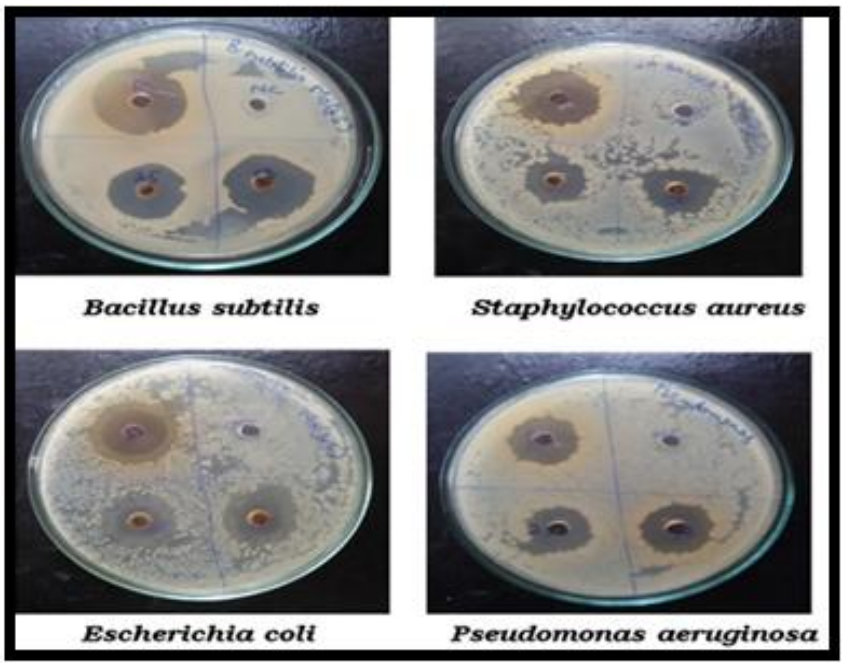

Fig.3.6. Antibacterial activity of MoO_3/Fe_2O_3/RGO nanocomposite.

Observed the antibacterial activity of MoO_3 nanobelts, MoO_3/Fe_2O_3 and MoO_3/Fe_2O_3/RGO ternary nanocomposite results (Fig.3.7), MoO_3/Fe_2O_3/RGO nanocomposite strongly inhibited the growth of Gram positive and Gram negative bacterial strains tested compared to MoO_3/Fe_2O_3 nanocomposite and MoO_3 nanobelts.

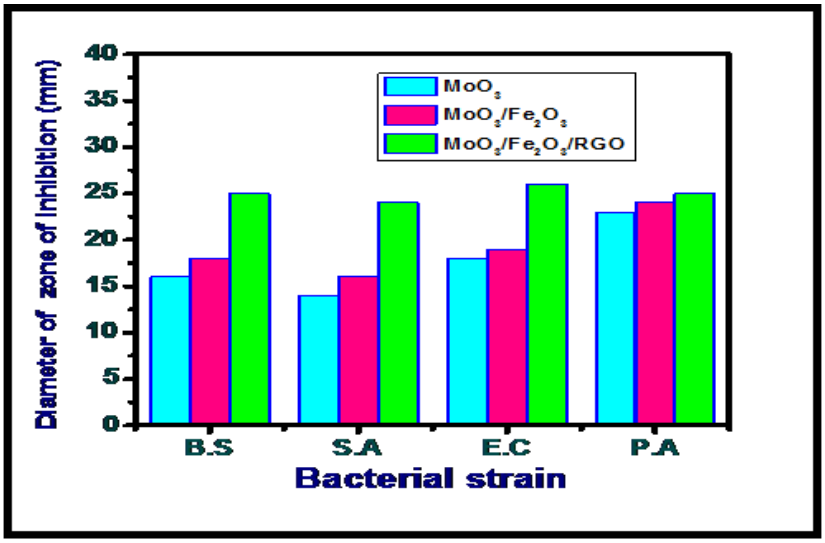

Fig.3.7. Diameter of zone of inhibition of MoO_3, MoO_3/Fe_2O_3 and MoO_3/Fe_2O_3/RGO on growth of Gram positive and Gram negative bacterial strain.

B.S: *Bacillus subtilis,* S.A: *Staphylococcus aureus,*

E.C: *Escherichia coli,* P.A: *Pseudomonas aeruginosa.*

5. Antibacterial mechanism of MoO_3/Fe_2O_3/RGO nanocomposite

The fabrication of reactive oxygen species (ROS) against microorganisms resulted in an antibacterial effect of metal oxide. This reaction occurs when particles are illuminated by light with energy higher than its band gap. In metal oxide, electrons obstacle from valence band to conduction band and formed negative charges (e^-) with positive electric-hole (h^+) pairs on catalyst surface. The positive electric-holes (h^+), forming hydroxyl free radicals, with a high oxidation power via absorbed water molecules are oxidized.[50] Likewise, negative charges react with the oxygen in water, producing superoxide radicals, ion homeostasis deregulation, coenzyme-independent respiration and cell wall structure disruption leading to cell death.[51,52] MoO_3/Fe_2O_3 nanocomposite onto graphene-based materials has in addition been considered. RGO layer decorated with MoO_3/Fe_2O_3 possess high antibacterial activity. As the interaction of bacteria with RGO is in addition dependent on the orientation of surface relative to the bacteria, the way RGO is deposited onto surfaces can influence the antimicrobial character significantly. The antibacterial mode of action of graphene such as production of reactive oxygen species[53], oxidative stress or vigorous extraction of large amounts of phospholipids from the membrane of the bacteria under consideration. And the bacterial cell death is caused by the leakage of sugars and proteins from the cell membrane once in contact with the MoO_3/Fe_2O_3/RGO ternary nanocomposite.[54]

6. CONCLUSION

In this paper MoO_3/Fe_2O_3 nanocomposite decorated on RGO lauyer was synthesized via hydrothermal process. The MoO_3/Fe_2O_3/RGO ternary nanocomposite was characterized by XRD, FTIR, SEM, EDX, TEM, Raman, UV-DRS and BET. The resulting ternary nanocomposite shows enhancive antibacterial activity when compared to binary nanocomposite and pure metal oxide against *Bacillus subtilis, Staphylococcus aureus, Escherichia coli* and *Pseudomonas aeruginosa*. Hence, considering above results theses ternary nanocomposite more useful in medical research and water purification process.

ACKNOWLEDGEMENT

The authors gratefully acknowledge to Council of Scientific and Industrial Research (CSIR), New Delhi, India for the financial support of this work and the Andhra University, Visakhapatnam, India authorities for extending cooperation in carrying out this work.

Conflicts of Interest

The authors declare that there is no conflict of interest.

REFERENCES

1. Q.L. Li, S. Mahendra, D.Y. Lyon, L. Brunet, M.V. Liga, D. Li, P.J.J. Alvarez, Antimicrobial nanomaterials for water disinfection and microbial control: potential applications and implications, Water Res., 2008; 42(18): 4591-4602.
2. D. Gangadharan, K. Harshvardan, G. Gnanasekar, D. Dixit, K.M. Popat, P.S.Anand, Polymeric microspheres containing silver nanoparticles as a bactericidal agent for water disinfection, Water Res., 2010; 44(180): 5481-5487.
3. Jennifer A. Dahl, Bettye L. S. Maddux, and James E. Hutchison, Toward Greener Nanosynthesis, Chem. Rev., 2007; 107(6): 2228–2269.
4. Zhang. L.; Jiang. Y.; Ding. Y.; Povey. M, York. D.; Investigation into the antibacterial behaviour of suspensions of ZnO nanoparticles (ZnO Nanofluids), J. Nanopart. Res., 2007; 9: 479-489.
5. Nagarajan, P.; Rajagopalan, V.; Enhanced bioactivity of ZnO nanoparticles-antimicrobial study, J. Sci. Technol. Adv. Mater, 2008; 9(3): 035004-035010.
6. Hajipour. M. J.; Fromm. K. M.; Ashkarran, A. A.; Aberasturi. D. J.; Larramendi. I. R.; Rojo. T.; Serpooshan. V.; Parak. W. J.; Mahmoodi, M., Antibacterial properties of nanoparticles, Trends Biotechno, 2012; 30(10): 499-511.

7. Donald G. Barceloux & Dr. Donald Barceloux, Molybdenum, Journal of Toxicology:Clinical Toxicology, 1999; 37(2): 231–237.
8. Gupta, U. C.; Gupta, S. C.; Trace element toxicity relationships to crop production and livestock and human health: implications for management, Communications in Soil Science and Plant Analysis, 1998; 29: 1491–1522.
9. Heijerick, D. G.; Regoli, L.; Stubblefield, W.; The chronic toxicity of molybdate to marine organisms. I. Generating reliable effects data, The Science of the Total Environment, 2012; 430: 260–269.
10. Kapp, R.; Molybdenum, Environmental Toxicology, 2005; 3: 145–148.
11. Gutbrod, K.; Zollfrank, C.; The photocataytic properties of Ti-Mo oxides prepared by a simple sol-gel route, Journal of Sol-Gel Science and Technology, 2013; 66: 111–119.
12. Allogho, G.; Ashrit, P. V.; Wettability and photochromic behaviour of molybdenum oxide thin films, Thin Solid Film, 2012; 520: 2326–2330.
13. Lorenz, K.; Bauer, S.; Gutbrod, K.; Guggenbichler, J. P.; Schmuki, P.; Zollfrank, C.; Anodic TiO_2 nanotube layers electrochemically filled with MoO_3 and their antimicrobial properties, Biointerphases, 2011; 6: 16–21.
14. Zollfrank, C.; Gutbrod, K.; Wechsler, P.; Guggenbichler, J. P.; The antimicrobial activity of transition metal acid MoO_3 prevents microbial growth on material surfaces, Materials Science and Engineering: C, 2012; 32: 47–54.
15. Guggenbichler, J. P.; Eberhardt, N.; Martinez, H. P.; Wildner, H, Substance With an Antimicrobial Effect, 2010; US 57199 A1.
16. Tétault, N.; Gbaguidi-Haore, H.; Bertrand, X.; Quentin, R.; Van der Mee-Marquet, N.; Biocidal activity of metalloacid-coated surfaces against multidrug-resistant microorganisms, Antimicrobial Resistance and Infection Control, 2012; 1: 35–42.
17. Lackner, M.; Maninger, S.; Guggenbichler, J. P.; Saure Oberflaechen als neuartige Kontaktbiozide, Nachrichten aus der Chemie, 2013; 61: 112–115.
18. Sun, B.; Sun, S. Q.; Li, T.; Zhang, W. Q.; Preparation and antibacterial activities of Ag-doped SiO_2–TiO_2 composite films by liquid phase deposition (LPD) method, J. Mater. Sci, 2007; 42(24): 10085–10089.
19. Shah, M.; Nag, M.; Kalagara, T.; Singh, S.; Manorama, S. V.; Silver on PEG-PU-TiO_2 polymer nanocomposite films: an excellent system for antibacterial applications, Chem. Mater., 2008; 20(7): 2455–2460.

20. Huanjun Zhang and Guohua Chen, Potent Antibacterial Activities of Ag/TiO_2 Nanocomposite Powders Synthesized by a One-Pot Sol−Gel Method, Environ. Sci. Technol, 2009; 43: 2905–2910.
21. O. Akhavan, E. Ghaderi, Self-accumulated Ag nanoparticles on mesoporous TiO_2thinfilm with high bactericidal activities, Surface & Coatings Technology, 2010; 204: 3676–3683.
22. O. Akhavan, Lasting antibacterial activities of Ag-TiO_2/Ag/a-TiO_2 nanocomposite thin film photocatalysts under solar light irradiation, Journal of Colloid and Interface Science, 2009; 336: 117–124.
23. Chockalingam Karunakaran, Paramasivan Gomathisankar, Govindasamy Manikandan, Preparation and characterization of antimicrobial Ce-doped ZnO nanoparticles for photocatalytic detoxification of cyanide, Materials Chemistry and Physics, 2010; 123: 585–594.
24. Cioffi, N.; Rai, M.; Nano-Antimicrobials: Progress and Prospects. Springer, 2012.
25. Lorenz, K.; Bauer, S.; Gutbrod, K.; Guggenbichler, J. P.; Schmuki, P.; Zollfrank, C.; Anodic TiO_2 nanotube layers electrochemically filled with MoO_3 and their antimicrobial properties, Biointerphases, 2011; 6: 16–21.
26. Hegab, H.M. et al, The controversial antibacterial activity of graphene-based materials, Carbon, 2016; 105: 362–376.
27. Hu, W. et al, Graphene-based antibacterial paper, ACS Nano., 2010; 4: 4317-4323.
28. Mejías Carpio, IE.; Santos, CM.; Wei, X. & Rodrigues, DF, Toxicity of a polymer-graphene oxide composite against bacterial planktonic cells, biofilms, and mammalian cells, Nanoscale, 2012; 4: 4746–4756.
29. Nguyen Bich, H. & Nguyen Van, H.; Promising applications of graphene and graphene-based nanostructures, Adv. Nat. Sci-Nanosci, 2016; 7.
30. Sundramoorthy, A. K. & Gunasekaran, S.; Applications of graphene in quality assurance and safety of food, Trends in Anal. Chem., 2014; 60: 36–53.
31. Pei, S. & Cheng, H.M.; The reduction of graphene oxide, Carbon, 2012; 50: 3210–3228.
32. T. S. Sreeprasad, S. M. Maliyekkal, K. P. Lisha and T. Pradeep, Reduced graphene oxide-metal/metal oxide composites: facile synthesis and application in water purification, J. Hazard. Mater, 2011; 186: 921–931.
33. J. Xu, L. Wang and Y. Zhu, Decontamination of bisphenol A from aqueous solution by graphene adsorption, Langmuir, 2012; 28: 8418–8425.

34. S. S. Gupta, T. S. Sreeprasad, S. M. Maliyekkal, S. K.Das and T. Pradeep, Graphene from sugar and its application in water purification, ACS Appl. Mater. Interfaces, 2012; 4: 4156–4163.
35. S. Wang, H. Sun, H. M. Ang and M. O. Tade, Adsorptive remediation of environmental pollutants using novel graphene-based nanomaterials, Chem. Eng. J, 2013; 226: 336–347.
36. Akhavan, O.; & Ghaderi, E.; Toxicity of graphene and graphene oxide nanowalls against bacteria, ACS Nano, 2010; 4: 5731–5736.
37. William S. Hummers Jr., Richard E. Offeman, Preparation of Graphitic Oxide, J. Am. Chem. Soc., 1958; 80: 1339–1339.
38. Murray, P.R.; Baron, E.J.; Pfaller, M.A.; Tenover, F.C. and Yolken, H.R.; Manual of Clinical Microbiology, 6th Edition, ASM Press, Washington DC, 1995; 15- 18.
39. Olurinola, PF, A laboratory manual of pharmaceutical microbiology, Idu, Abuja, Nigeria, 1996; 69-105.
40. Elizabeth, M.; Adrien Szekely Johnson.; David, W.; and Warnock, Comparison of E-Test and Broth. Microdilution. Methods for Antifungal. Drug. Susceptibility Testing of Molds, J. Clin. Microbiol, 1999; 37(5): 1480-1483.
41. Y. Zhao, X. Song, Q. Song and Z. Yin, A facile route of the synthesis copper oxide/reduced graphene oxide nanocomposites and electrochemical detection of catechol organic pollutant, Cryst. Eng. Comm., 2012; 14: 6710-6719.
42. Cai L, Rao P M and Zheng X L, Morphology-controlled flame synthesis of single, branched, and flower-like a-MoO_3 nanobelt arrays, Arrays Nano Lett., 2011; 11: 872–877.
43. C. Nethravathi and M. Rajamathi, The production of smectite clay/graphene composites through delamination and costacking, Carbon, 2008; 46: 1994–1998.
44. J. S. Park, S. M. Cho, W. J. Kim, J. Park and P. J. Yoo, Fabrication of graphene thin films based on layer-by-layer self-assembly of functionalized graphene nanosheets, ACS Appl. Mater. Interfaces, 2011; 3: 360–368.
45. Chien-Tsung W, Photocatalytic activity of nanoparticle gold/iron oxideaerogels for azo dye degradation, J. Non-Cry. Solids, 2007; 353: 1126-1133.
46. Y. Xia and L. Yin, Core–shell structured α-Fe_2O_3@TiO_2 nanocomposites with improved photocatalytic activity in the visible light region, Phys. Chem. Chem. Phys., 2013; 15: 18627–18634.

47. Peng, L.; Xie, T.; Lu, Y.; Fan, H.; and Wang, D, Synthesis, photoelectric properties and photocatalytic activity of the Fe_2O_3/TiO_2 heterogeneous photocatalysts, Phys. Chem. Chem. Phys, 2010; 12: 8033– 8041.
48. S. Sakthivel and H. Kisch, Daylight photocatalysis by carbon-modified titanium dioxide, Angew. Chem., Int. Ed, 2003; 42: 4908–4911.
49. Y. Hou, F. Zuo, A. Dagg and P. Feng, Visible light-driven α-Fe_2O_3 nanorod/graphene/$BiV_{1-x}Mo_xO_4$ core/shell heterojunction array for efficient photoelectrochemical water splitting, Nano Lett., 2012; 12: 6464–6473.
50. Trunina N. A.; M. E. Darvin, K. Kord´as et al, IEEE Journal of Selected Topics in Quantum Electronics, 2014; 20(3): 133–140.
51. Kubacka A, Diez MS, Rojo D, Bargiela R, Ciordia S, Zapico I, Albar JP, Barbas C, Matrins dos Santos VAP, Fernandez-Garcia M, Understanding the antimicrobial mechanism of TiO_2-based nanocomposite films in a pathogenic bacterium, Scientific Reports, 2014; 4(4134): 1-9.
52. Wan, Y. et al, Vancamycin-functionalised Ag@TiO_2 phototoxicity for bacteria, J. Hazard. Mater, 2011; 186: 306–312.
53. K. Krishnamoorthy, M. Veerapandian, L. H. Zhang, K. Yun and S. J. Kim, Antibacterial efficiency of graphene nanosheets against pathogenic bacteria via lipid peroxidation, J. Phys. Chem. C, 2012; 116: 17280–17287.
54. N. Hussain, A. Gogoi, R. K. Sarma, P. Sharma, A. Barras, R. Boukherroub, R. Saikia, P. Sengupta and M. R. Das, Reduced graphene oxide nanosheets decorated with Au nanoparticles as an effective bactericide: Investigation of biocompatibility and leakage of sugars and proteins, Chem Plus Chem, 2014; 79: 1774–1784.